Supplementary information: Enhancing the performance of hard carbon for sodium-ion batteries by coating with silicon nitride/oxycarbide nanoparticles

Hang Cheng, Nuria Garcia-Araez, and Andrew L. Hector*

School of Chemistry, University of Southampton, Southampton SO17 1BJ, United Kingdom

Fig. S1 First cycle charge-discharge capacity curves (sodium half-cells with 1 mol dm^{-3} $NaClO_4$ in EC/DEC electrolyte using a current of 50 mA g^{-1}) of composites of hard carbon with (a) silicon nitride and (b) silicon carbide produced by reacting cellulose with different volumes of silicon chloride (as labelled) and firing under nitrogen or argon at 1400 °C.

Fig. S2 XRD patterns of HC-SiOC-0.4 composites obtained at 1200 and 1400 °C.

Fig. S3 TGA and differential TGA results of (a) HC-SiN_x-0.4 and (b) HC-SiOC-0.4 composites. The gas mixture was Ar (50 mL min^{-1}) and O_2 (20 mL min^{-1}) and the heating rate was 4 °C min^{-1}.

Fig. S4 Raman spectra of hard carbon composites with (a) silicon nitride and (b) silicon oxycarbide, showing spectra for the highest loading composites made to highlight the presence of features due to Si-N and Si-C bonds. Broken lines highlight the presence of features due to Si-N and Si-C bonds.

Fig. S5 Raman spectra of hard carbon composites with with (a) silicon nitrides and (b) silicon oxycarbides with loadings as labelled.

Fig. S6 Typical Raman spectrum fitting of HC-SiN_x-0.4 composite.

Fig. S7 Nitrogen adsorption-desorption isotherms of hard carbon composites with (a) silicon nitrides and (b) silicon oxycarbides with loadings as labelled.

Fig. S8 Pore size distribution of hard carbon coated with (a) silicon nitride and (b) silicon oxycarbide with loadings as labelled, calculated using the DFT method.

Fig. S9 The survey spectra of HC-SiN_x-0.4 and HC-SiOC-0.4 electrodes.

Fig. S10 Si 2p spectra of (a) HC-SiN_x-0.4 and (b) HC-SiOC-0.4 electrodes after sodiation (sodium half-cells with 1 mol dm^{-3} $NaClO_4$ in EC/DEC electrolyte using a current of 50 mA g^{-1}) with no Ar^+ etching.

Fig. S11 N 1s spectrum of HC-SiN_x-0.4 electrodes after sodiation (sodium half-cells with 1 mol dm^{-3} $NaClO_4$ in EC/DEC electrolyte using a current of 50 mA g^{-1}) and Ar^+ etching for 5 min.

Fig. S12 First cycle differential capacity plots (sodium half-cells with 1 mol dm^{-3} $NaClO_4$ in EC/DEC electrolyte using a current of 50 mA g^{-1}) of hard carbon composites with (a) silicon nitride and (b) silicon oxycarbide with loadings as labelled.

Fig. S13 Enlarged view of the differential capacity plots shown in Fig. S12 in the 0-0.5 V voltage region.

Fig. S14 Enlarged view of differential capacity plots (sodium half-cells with 1 mol dm^{-3} $NaClO_4$ in EC/DEC electrolyte using a current of 50 mA g^{-1}) of (a) HC-SiN_x-0.4 and (b) HC-SiOC-0.4, for different cycles, as labelled.

Fig. S15 Enlarged view of differential capacity plots (sodium half-cells with 1 mol dm^{-3} $NaClO_4$ in EC/DEC electrolyte using a current of 50 mA g^{-1}) of (a) HC-N_2 and (b) HC-Ar, for different cycles, as labelled.

Fig. S16 Nyquist plots (frequency range from 0.05 Hz to 500 kHz, at open circuit potential with the electrode in the oxidised condition) of (a) HC-SiN_x-0.4 and (b) HC-SiOC-0.4, before and after 50 cycles (sodium half-cells with 1 mol dm^{-3} $NaClO_4$ in EC/DEC electrolyte using a current of 50 mA g^{-1} and a potential range of 2V – 5 mV).

Fig. S17 Nyquist plots (frequency range from 0.05 Hz to 500 kHz, at open circuit potential with the electrode in the oxidised condition) of (a) HC-N_2 and (b) HC-Ar, before and after 50 cycles (sodium half-cells with 1 mol dm^{-3} $NaClO_4$ in EC/DEC electrolyte using a current of 50 mA g^{-1} and a potential range of 2V – 5 mV).

Fig. S18 The C 1s depth profile of (a) HC-SiN_x-0.4 and (b) HC-SiOC-0.4 composites after first discharging (sodium half-cells with 1 mol dm^{-3} $NaClO_4$ in EC/DEC electrolyte using a current of 50 mA g^{-1}) as a function of Ar-ion etch time.

Fig. S19 C1s spectra of (a) HC-SiN_x-0.4 and (b) HC-SiOC-0.4 electrodes sodiated in 1 mol dm^{-3} $NaClO_4$ in EC/DEC electrolyte. Measurements at various depths by Ar^+ sputtering.

Equation S1 Reaction equations for carbothermal formation of silicon nitride and silicon carbide.

Table S1 Comparison of sodium storage performance between HC-SiNx-0.4 and previously reported hard carbons.

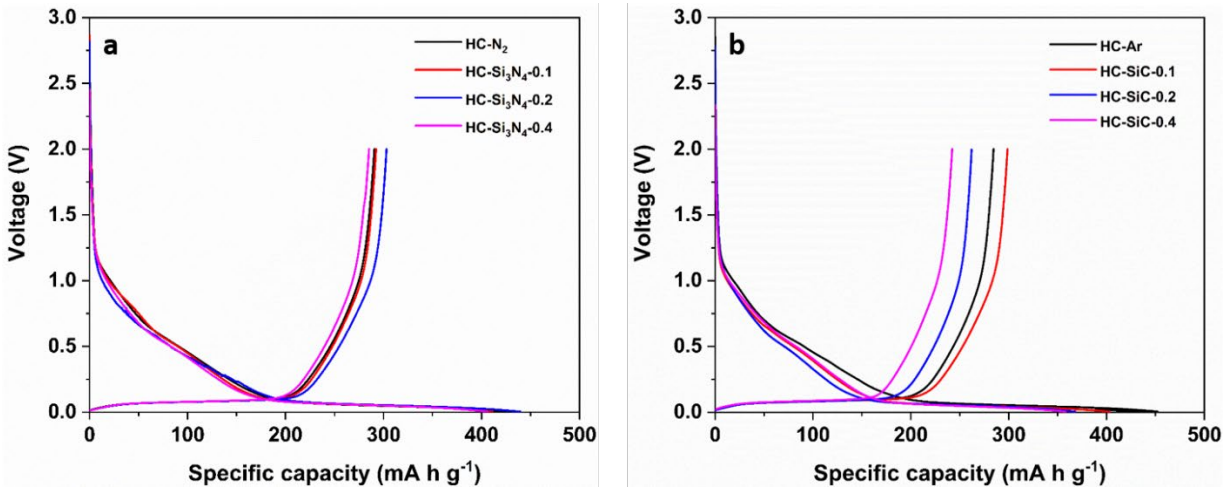

Fig. S1 First cycle charge-discharge capacity curves (sodium half-cells with 1 mol dm^{-3} $NaClO_4$ in EC/DEC electrolyte using a current of 50 mA g^{-1}) of composites of hard carbon with (a) silicon nitride and (b) silicon carbide produced by reacting cellulose with different volumes of silicon chloride (as labelled) and firing under nitrogen or argon at 1400 °C.

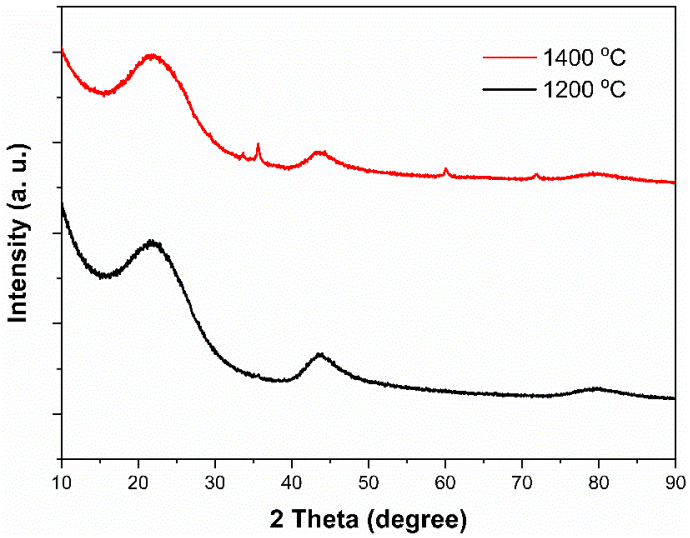

Fig. S2 XRD patterns of HC-SiOC-0.4 composites obtained at 1200 and 1400 °C.

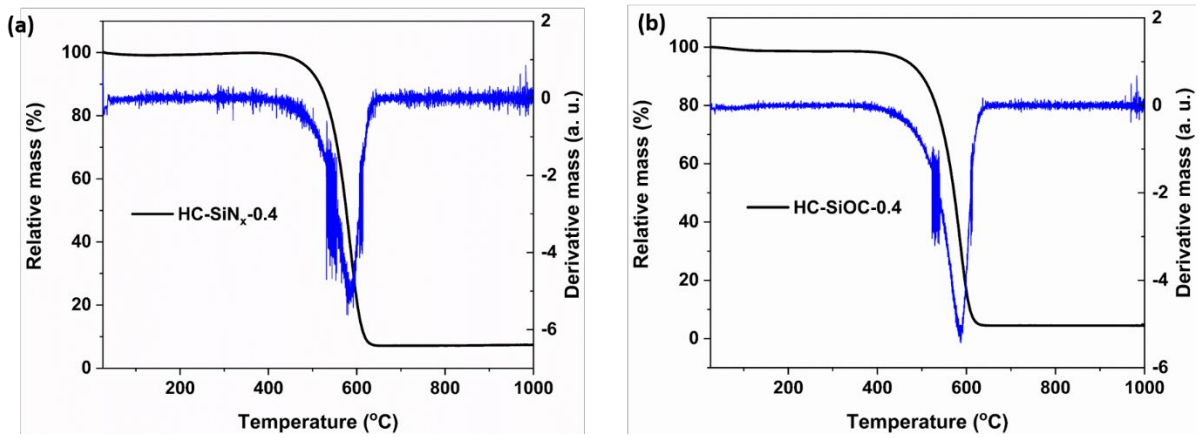

Fig. S3 TGA and differential TGA results of (a) HC-SiN_x-0.4 and (b) HC-SiOC-0.4 composites. The gas mixture was Ar (50 mL min^{-1}) and O_2 (20 mL min^{-1}) and the heating rate was 4 °C min^{-1}.

Table S1. Residual mass (wt%) in TGA measurements

Sample	Residual mass (wt%)
HC-SiN_x-0.1	5.93
HC-SiN_x-0.2	6.47
HC-SiN_x-0.4	8.92
HC-SiN_x-0.8	13.43
HC-SiOC-0.1	5.10
HC-SiOC-0.2	5.21
HC-SiOC-0.4	5.80
HC-SiOC-0.8	6.59

Estimation of the silicon nitride and oxycarbide content from thermogravimetric analysis

The residual mass after the sample was combusted in the TGA was 8.92% for the HC-SiN_x-0.4 composite and 5.80% for HC-SiOC-0.4. Due to the possibility that the silicon species do not fully oxidise the residual mass would be expected to be in a range between the following values:

1) Taking the mass of HC-SiN_x-0.4 composite as "m", and the mass proportion of Si_3N_4 in the composite as "x", considering the combustion reaction (1a), the expected mass of SiO_2 remaining after combustion would be 180.27mx/140.27, from which the value of x (that is, the Si_3N_4 mass content) is found to be 6.94%. Considering a nitrogen-deficient silicon nitride such as SiN, following the same type of calculations gives a value of x of 6.25%. For the HC-SiOC-0.4 composite, similar calculations give a SiC or SiOC mass content in the sample of 3.87 or 5.41%.

$$aC + bSi_3N_4 + (\mathrm{a} + 7\mathrm{b})\mathrm{O}_2 \rightarrow 3bSiO_2 + 4bNO_2 + aCO_2 \quad (1a)$$

$$aC + bSiN + (\mathrm{a} + 2\mathrm{b})\mathrm{O}_2 \rightarrow bSiO_2 + bNO_2 + aCO_2 \quad (1b)$$

$$aC + bSiC + (a + 2b)O_2 \rightarrow bSiO_2 + (a + b)CO_2 \quad (2a)$$

$$aC + bSiOC + (a + \tfrac{3}{2}b)O_2 \rightarrow bSiO_2 + (a + b)CO_2 \quad (2b)$$

2) If we consider the reactions in which the carbon is combusted but the silicon nitride or (oxy)carbide is unchanged (equations 3&4), the mass content of silicon nitride or (oxy)carbide is found to be 8.92% in HC-SiN_x-0.4 and 5.80% in HC-SiOC-0.4.

$$aC + bSi_3N_4 + \mathrm{a}\mathrm{O}_2 \rightarrow bSi_3N_4 + aCO_2 \quad (3a)$$

$$aC + bSiN + \mathrm{a}\mathrm{O}_2 \rightarrow bSiN + aCO_2 \quad (3b)$$

$$aC + bSiC + aO_2 \rightarrow bSiC + aCO_2 \quad (4a)$$

$$aC + bSiOC + aO_2 \rightarrow bSiOC + aCO_2 \quad (4b)$$

In table 1, we report the average and standard deviation of the estimations of the SiN_x or SiOC content in the samples obtained considering reactions 1b and 3, and reactions 2a and 4, since the results with reactions 1a and 2b lie in between these two extreme scenarios.

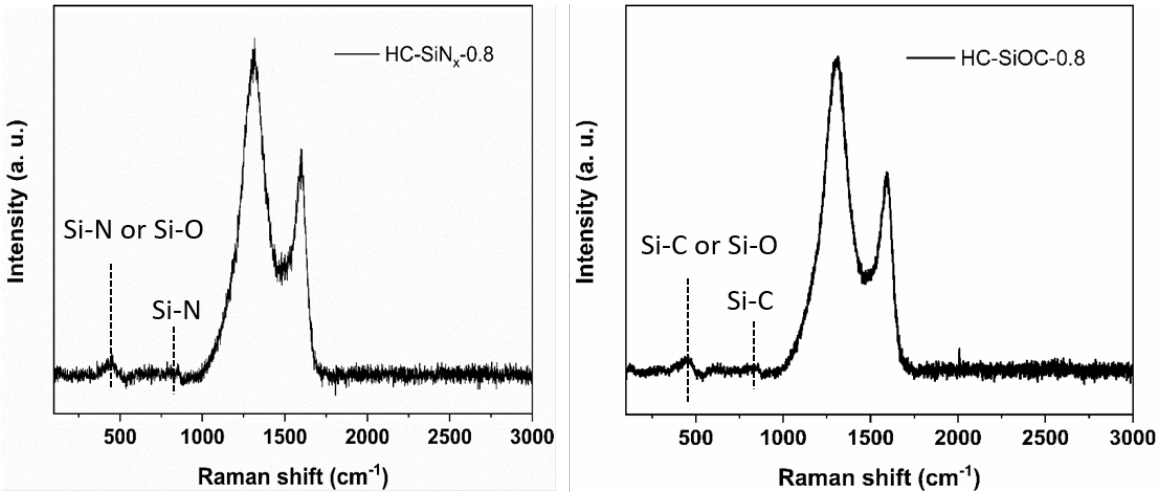

Fig. S4 Raman spectra of hard carbon composites with (a) silicon nitride and (b) silicon oxycarbide, showing spectra for the highest loading composites. Broken lines highlight the presence of features due to Si-N and Si-C bonds.

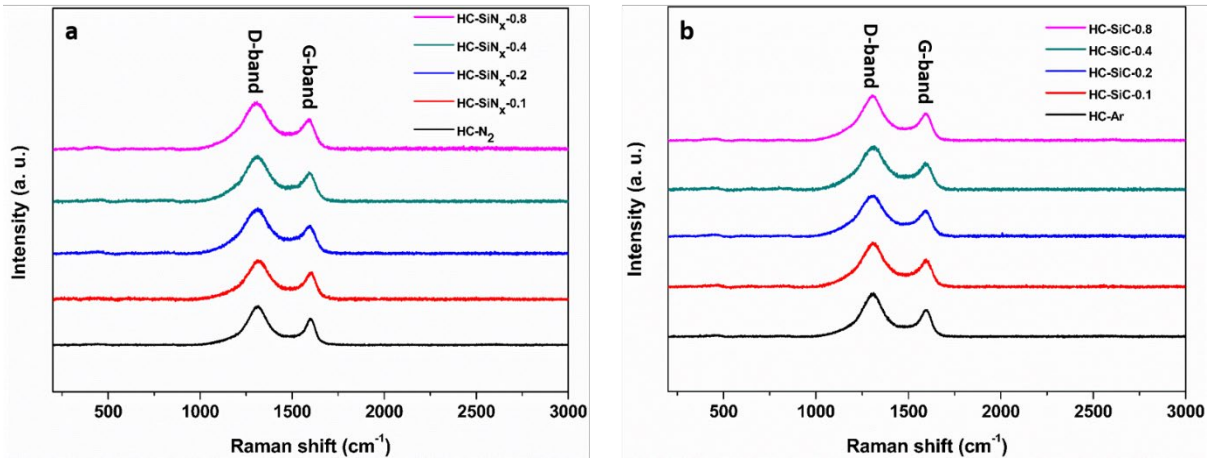

Fig. S5 Raman spectra of hard carbon composites with (a) silicon nitride and (b) silicon oxycarbide with loadings as labelled.

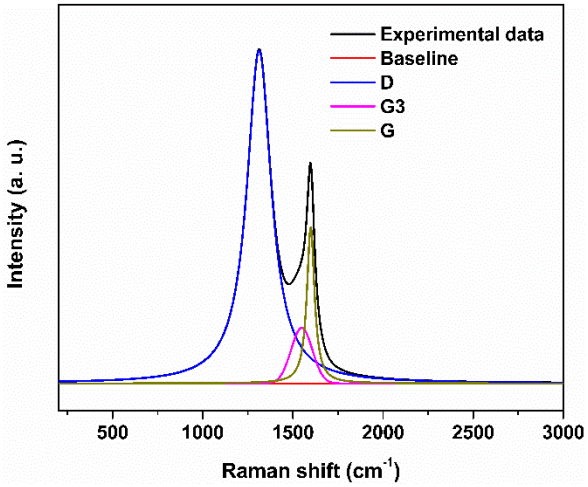

Fig. S6 Typical Raman spectrum fitting for the HC-SiN_x-0.4 composite.

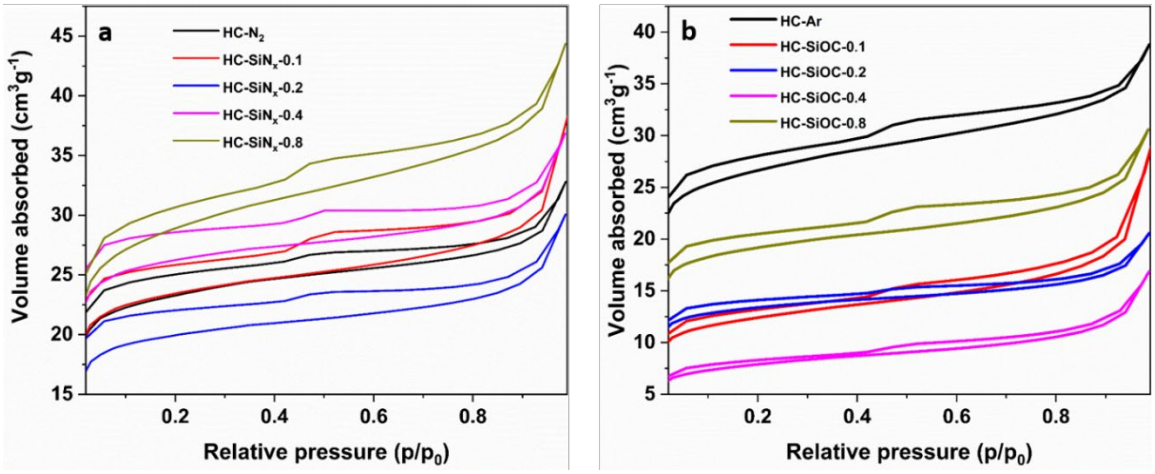

Fig. S7 Nitrogen adsorption-desorption isotherms of hard carbon composites with (a) silicon nitride and (b) silicon oxycarbide with loadings as labelled.

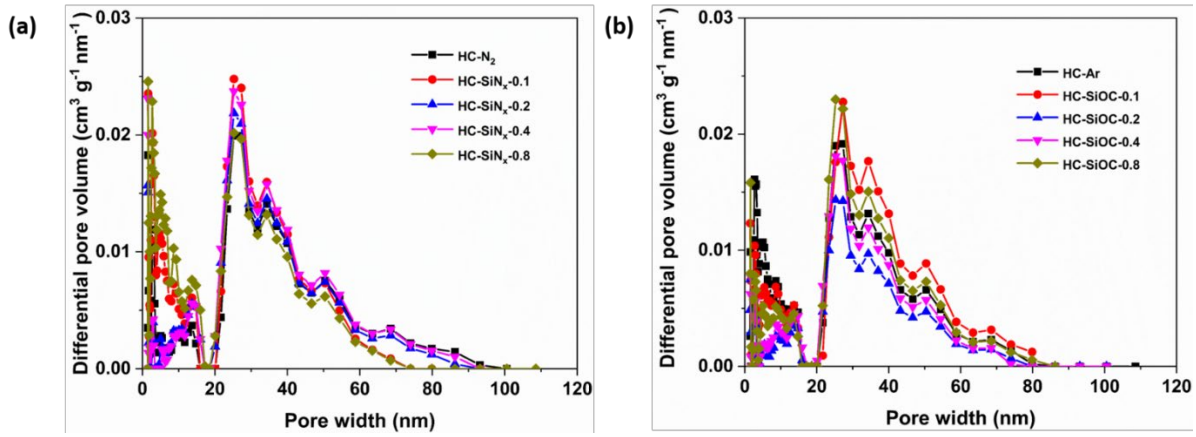

Fig. S8 Pore size distribution of hard carbon coated with (a) silicon nitride and (b) silicon oxycarbide with loadings as labelled, calculated using the DFT method.

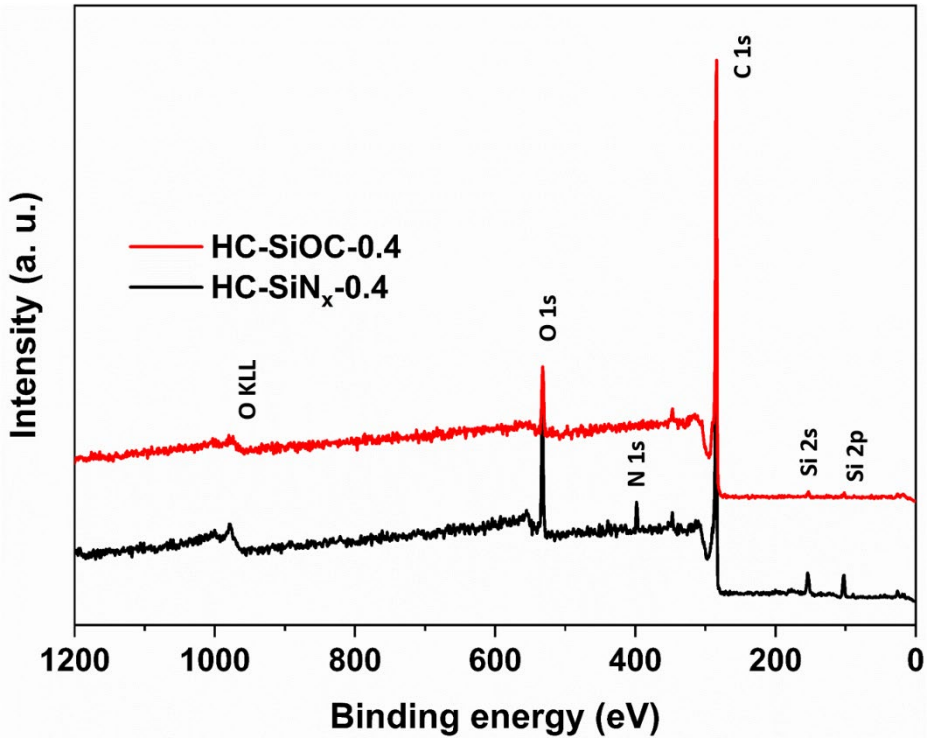

Fig. S9 The survey spectra of HC-SiN$_x$-0.4 and HC-SiOC-0.4 electrodes.

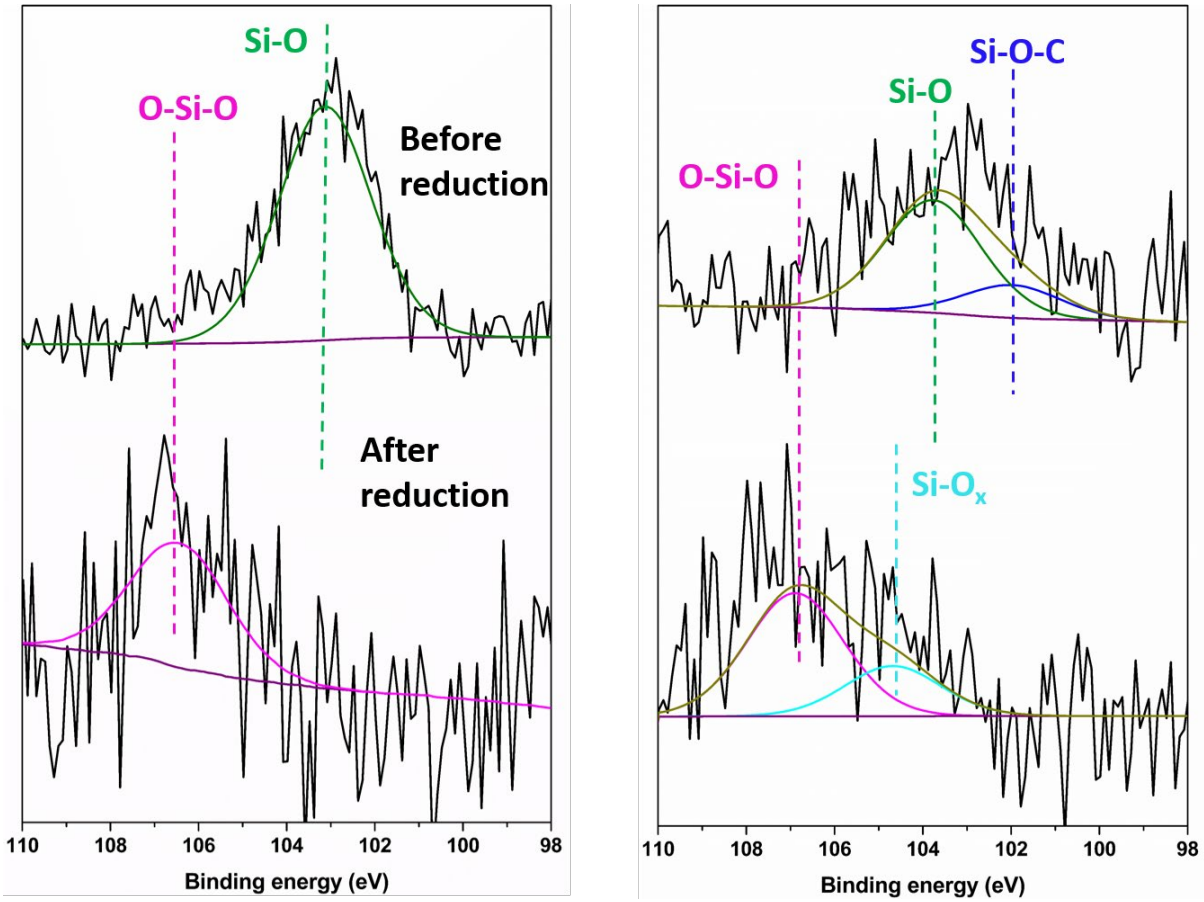

Fig. S10 Si 2p spectra of (a) HC-SiN$_x$-0.4 and (b) HC-SiOC-0.4 electrodes before and after reduction in sodium half-cells with 1 mol dm^{-3} NaClO$_4$ in EC/DEC electrolyte using a current of 50 mA g^{-1}, with no Ar$^+$ etching prior to the XPS measurements.

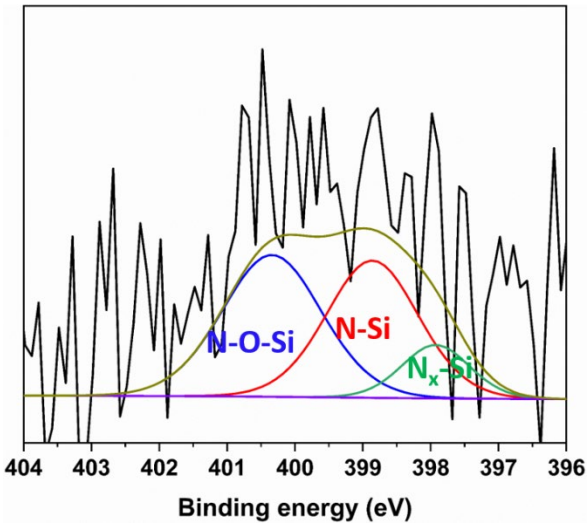

Fig. S11 N 1s spectrum of HC-SiN$_x$-0.4 electrodes after reduction in sodium half-cells with 1 mol dm^{-3} NaClO$_4$ in EC/DEC electrolyte using a current of 50 mA g^{-1}, and Ar$^+$ etching for 5 min prior to the XPS measurements.

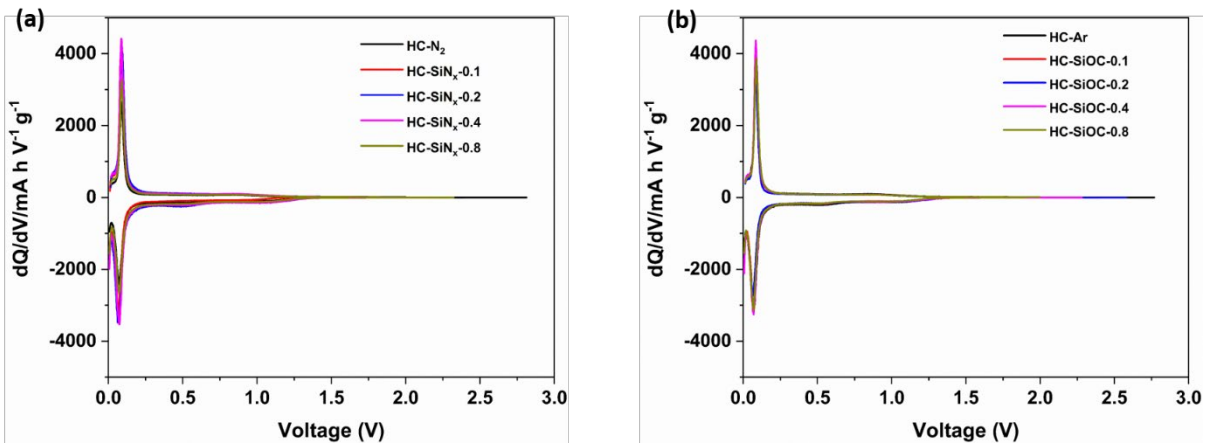

Fig. S12 First cycle differential capacity plots (sodium half-cells with 1 mol dm^{-3} $NaClO_4$ in EC/DEC electrolyte using a current of 50 mA g^{-1}) of hard carbon composites with (a) silicon nitride and (b) silicon oxycarbide with loadings as labelled.

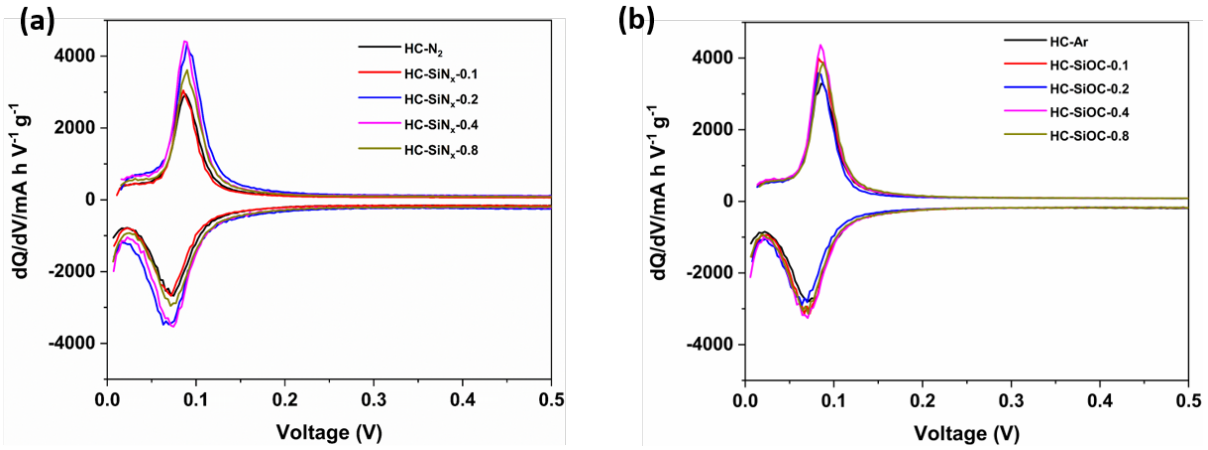

Fig. S13 Enlarged view of the differential capacity plots shown in figure S12 in the 0-0.5 V voltage region.

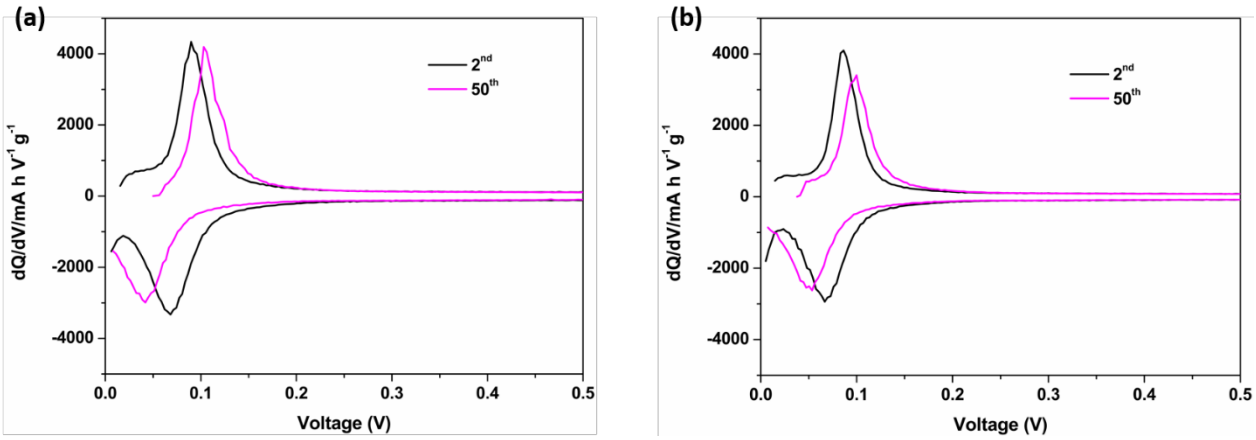

Fig. S14 Enlarged view of differential capacity plots (sodium half-cells with 1 mol dm^{-3} $NaClO_4$ in EC/DEC electrolyte using a current of 50 mA g^{-1}) of (a) HC-SiN_x-0.4 and (b) HC-SiOC-0.4, for different cycles, as labelled.

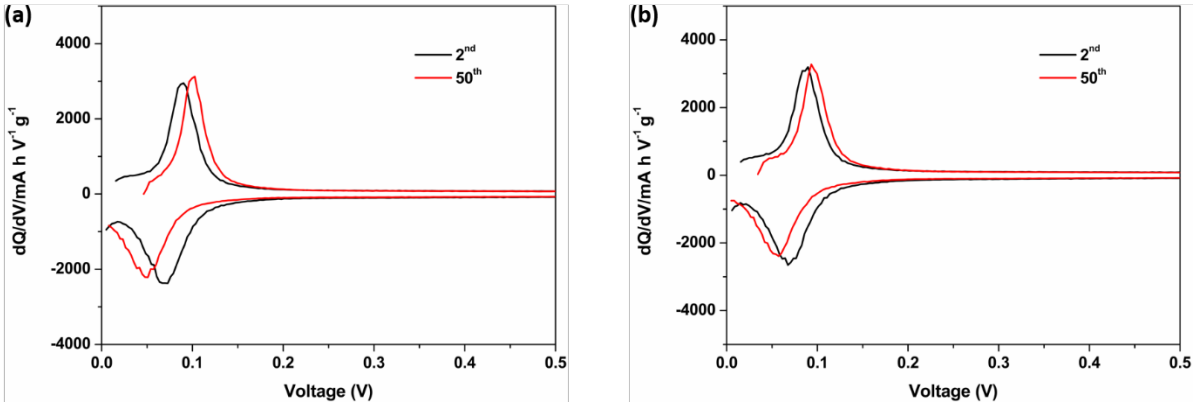

Fig. S15 Enlarged view of differential capacity plots (sodium half-cells with 1 mol dm^{-3} $NaClO_4$ in EC/DEC electrolyte using a current of 50 mA g^{-1}) of (a) HC-N_2 and (b) HC-Ar, for different cycles, as labelled.

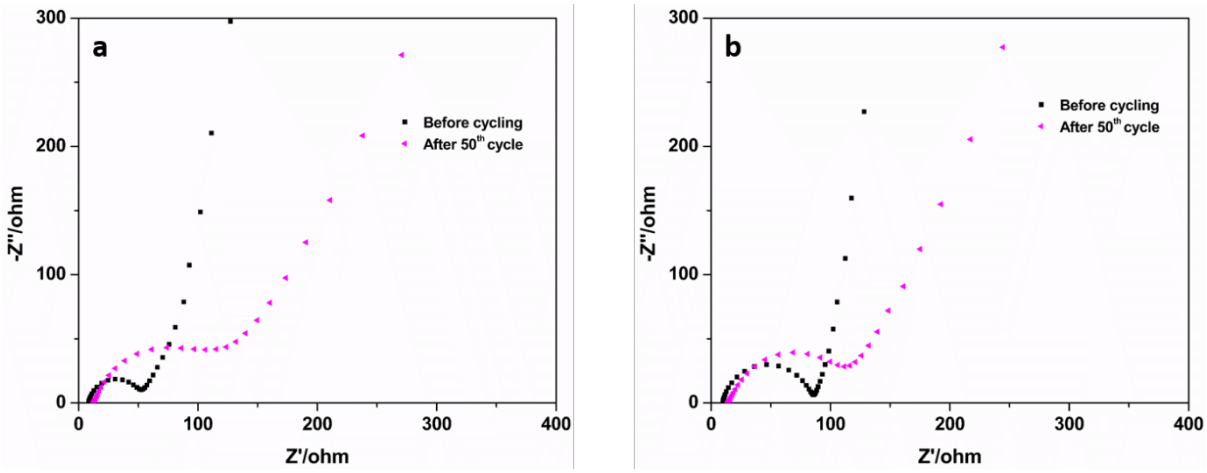

Fig. S16 Nyquist plots (frequency range from 0.05 Hz to 500 kHz, at open circuit potential with the electrode in the oxidised condition) of (a) HC-SiN_x-0.4 and (b) HC-SiOC-0.4, before and after 50 cycles (sodium half-cells with 1 mol dm^{-3} $NaClO_4$ in EC/DEC electrolyte using a current of 50 mA g^{-1} and a potential range of 2V – 5 mV).

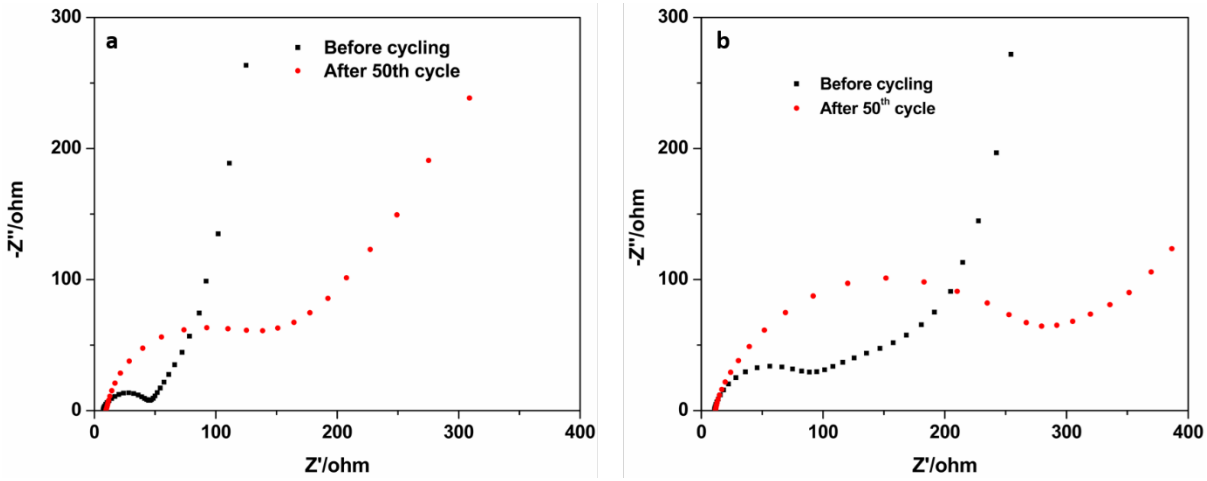

Fig. S17 Nyquist plots (frequency range from 0.05 Hz to 500 kHz, at open circuit potential with the electrode in the oxidised condition) of (a) HC-N_2 and (b) HC-Ar, before and after 50 cycles (sodium half-cells with 1 mol dm^{-3} $NaClO_4$ in EC/DEC electrolyte using a current of 50 mA g^{-1} and a potential range of 2V – 5 mV).

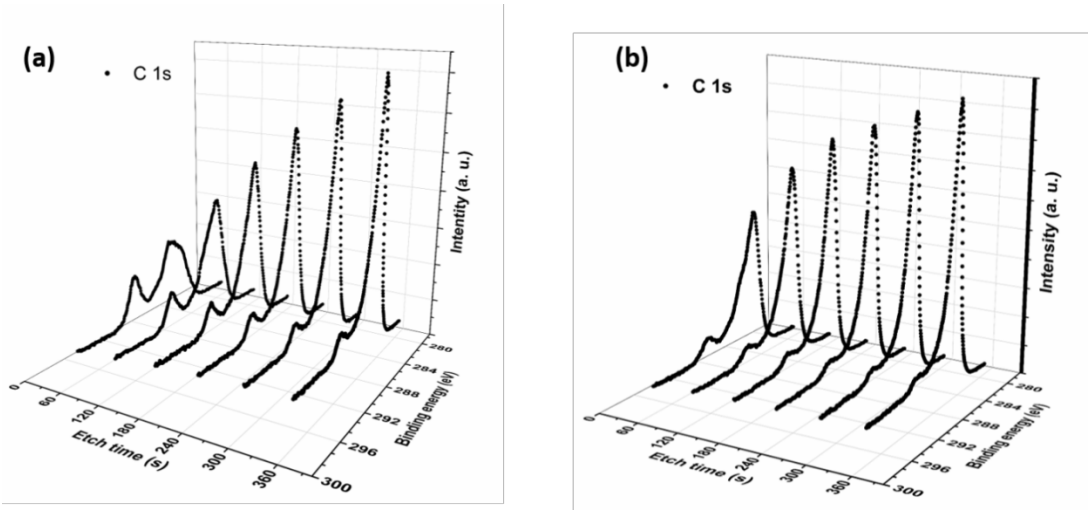

Fig. S18 The C 1s depth profile of (a) HC-SiN_x-0.4 and (b) HC-SiOC-0.4 composites after the first reduction in sodium half-cells with 1 mol dm^{-3} $NaClO_4$ in EC/DEC electrolyte using a current of 50 mA g^{-1}, as a function of Ar-ion etch time.

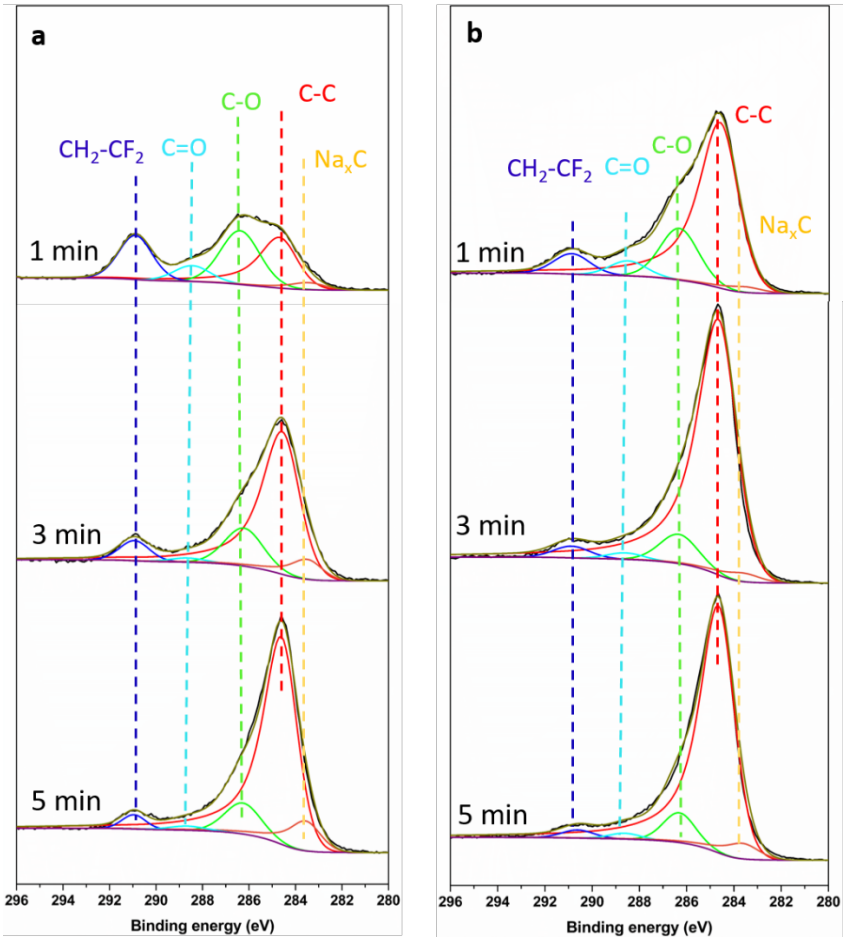

Fig. S19 C1s spectra of (a) HC-SiN_x-0.4 and (b) HC-SiOC-0.4 electrodes sodiated in 1 mol dm^{-3} $NaClO_4$ in EC/DEC electrolyte. Measurements at various depths by Ar^+ sputtering.

$$SiO_2 + \frac{2}{3}N_2 + 2C \rightarrow \frac{1}{3}Si_3N_4 + 2CO \quad (1)$$

$$SiO_2 + 2C \rightarrow SiOC + CO \quad (2)$$

Equation S1 Suggested possible reactions for carbothermal formation of silicon nitride and silicon (oxy)carbide.

Table S2 Comparison of sodium storage performance between HC-SiNx-0.4 and previously reported hard carbons.

Materials	Precursor	Mas loading (mg cm^{-2})	Electrolyte	Voltage window	Oxidation capacity	ICE(%)	Reference
HC-SiNx-0.4	Cotton wool	2-2.5, Swagelok cells	1 M $NaClO_4$ in EC/DEC	0.005-2 V	351 mA h g^{-1} at 50 mA g^{-1}	69	This work
Hard carbon	Apple	0.97-1.05, Swagelok cells	1 M $NaClO_4$ in EC/PC	0.02-3 V	230 mA h g^{-1} at 20 mA g^{-1}	61	[1]
Carbon nanofibers	Cellulose nanofibres	1-1.2, coin cells (CR2032)	1 M $NaClO_4$ in EC/PC	0.01-2 V	255 mA h g^{-1} at 40 mA g^{-1}	58.8	[2]
Carbon membranes	Leaf	N/A, coin cells (CR2032)	1 M $NaClO_4$ in EC/DEC	0-2.5 V	270 mA h g^{-1} at 40 mA g^{-1}	74.8	[3]
Carbon nanotubes	Cotton	2.5-3.5, coin cells (CR2032)	0.8 M $NaPF_6$ in EC/DMC	0-2 V	315 mA h g^{-1} at 30 mA g^{-1}	83	[4]
Carbon sheets	stalks	N/A, coin cells (CR2032)	1 M $NaClO_4$ in EC/DEC	0.01-3 V	260 mA h g^{-1} at 100 mA g^{-1}	52.6	[5]
Carbon nanosheets	Peat moss	~1, coin cells (CR2032)	1 M $NaClO_4$ in EC/DEC	0.001-2.8 V	298 mA h g^{-1} at 50 mA g^{-1}	57.5	[6]
Hard carbon	Switchgrass	0.5, coin cells (CR2025)	1 M $NaClO_4$ in EC/DEC	0.01-2 V	298 mA h g^{-1} at 50 mA g^{-1}	64	[7]
Actived hard cabron	Argan shells	1.2-2, coin cells (CR2032)	1 M $NaPF_6$ in EC/DEC	0-2 V	333 mA h g^{-1} at 50 mA g^{-1}	79.0	[8]
Hard carbon	Peanut shells	~1.5, coin cells (CR2025)	1 M $NaClO_4$ in EC/PC	0.001-2 V	261 mA h g^{-1} at 100 mA g^{-1}	58±2	[9]
3D free-standing hard carbon	hemp haulm	N/A, coin cells (CR2032)	0.8 M $NaClO_4$ in DMC	0.01-3 V	256 mA h g^{-1} at 37.4 mA g^{-1}	N/A	[10]
Hard carbon	Lotus seedpod	N/A, coin cells (CR2025)	1 M $NaClO_4$ in PC with 2% FEC	0.01-2.5 V	328.8 mA h g^{-1} at 50 mA g^{-1}	50.4	[11]

References

1. L. Wu, D. Buchholz, C. Vaalma, G. A. Giffin and S. Passerini, *ChemElectroChem*, 2016, **3**, 292-298.
2. W. Luo, J. Schardt, C. Bommier, B. Wang, J. Razink, J. Simonsen and X. Ji, *J. Mater. Chem. A*, 2013, **1**, 10662-10666.
3. H. Li, F. Shen, W. Luo, J. Dai, X. Han, Y. Chen, Y. Yao, H. Zhu, K. Fu, E. Hitz and L. Hu, *ACS Appl. Mater. Interfaces*, 2016, **8**, 2204-2210.
4. Y. Li, Y.-S. Hu, M.-M. Titirici, L. Chen and X. Huang, *Adv. Energy Mater.*, 2016, **6**, 1600659-1600667.
5. D. Qin, F. Zhang, S. Dong, Y. Zhao, G. Xu and X. Zhang, *RSC Adv.*, 2016, **6**, 106218-106224.
6. J. Ding, H. Wang, Z. Li, A. Kohandehghan, K. Cui, Z. Xu, B. Zahiri, X. Tan, E. M. Lotfabad, B. C. Olsen and D. Mitlin, *ACS Nano*, 2013, **7**, 11004-11015.
7. F. Zhang, Y. Yao, J. Wan, D. Henderson, X. Zhang and L. Hu, *ACS Appl. Mater. Interfaces*, 2017, **9**, 391-397.
8. M. Dahbi, M. Kiso, K. Kubota, T. Horiba, T. Chafik, K. Hida, T. Matsuyama and S. Komaba, *J. Mater. Chem. A*, 2017, **5**, 9917-9928.
9. X. Ren, S.-D. Xu, S. Liu, L. Chen, D. Zhang and L. Qiu, *J. Electroanal. Chem.*, 2019, **841**, 63-72.
10. P. Wang, K. Zhu, K. Ye, Z. Gong, R. Liu, K. Cheng, G. Wang, J. Yan and D. Cao, *J. Colloid Interface Sci.*, 2020, **561**, 203-210.
11. F. Wu, M. Zhang, Y. Bai, X. Wang, R. Dong and C. Wu, *ACS Appl. Mater. Interfaces*, 2019, **11**, 12554-12561.